Estimating Interfacial Tension via Relaxation of Drop Shapes and Filament Breakup

Mahari Tjahjadi and Julio M. Ottino
Dept. of Chemical Engineering, Northwestern University, Evanston, IL 60208

Howard A. Stone
Div. of Applied Sciences, Harvard University, Cambridge, MA 02138

Two methods are presented for calculating the interfacial tension between two immiscible Newtonian fluids. The procedures require only two measurements of the approximate interface shape during the low-Reynolds-number interfacial-tension-driven transient motion of (i) the relaxation of a modestly elongated drop back to a spherical shape or (ii) the growth of capillary wave instabilities along the surface of a thread. The interfacial tension can be estimated by comparing the time differences between the two experimental measurements with tabulated and numerically generated results for the approximate shape evolution. The numerical results are generated using the boundary integral method for similar model free-boundary problems at low Reynolds numbers. The tabulated results are presented for drop to suspending fluid viscosity ratios 0.01 to 10.

Introduction

There are a wide variety of techniques available for measuring the surface tension between a liquid and air (Adamson, 1990). Common laboratory procedures include capillary rise, the du Noüy ring, and the Wilhelmy slide techniques. Each of these methods depends on a balance of the surface tension force against the gravitational force acting on the deformed fluid surface. Alternatively, several methods are available for determining the surface tension from measurements of the equilibrium shape of bubbles and drops; for example, pendant and sessile drop methods, and the spinning drop tensiometer (Joseph et al., 1992). These methods have been also used to measure the interfacial tension for liquid-liquid interfaces.

The standard methods mentioned above require an accurate measurement of the density difference and/or waiting the required time for attainment of an equilibrium shape. Consequently, the techniques involve significant errors when determining the interfacial tension between nearly neutrally buoyant fluids or between very viscous fluids which take a long time to attain an equilibrium shape.

Another possibility for determining the interfacial tension is to use dynamic methods which follow the transient evolution. Such an approach was recently taken by Carriere et al. (1989) who described the interfacial-tension-driven motion of an initially stretched fluid drop relaxing back to a spherical shape and Elemans et al. (1990) who described the capillary instability and breakup of a long fluid filament, which they called the "breaking thread" method. In each experiment, the fluid-fluid interface changes shape as a function of time, and simple models were introduced from which to estimate the interfacial tension given observations of the shape evolution.

The drop retraction method can be traced back to the work of Taylor (1934) who estimated interfacial tension by comparing the steady-state shape of nearly spherical neutrally buoyant drops, deformed in a viscous simple shear or extensional flow, with a theoretical prediction for small drop deformations. This idea has been used by a number of researchers (for example, Rumscheidt and Mason, 1961; Bentley and Leal, 1986), though is somewhat limited in practice since it requires that a drop be placed in a carefully controlled flow. The novel feature of the method described by Carriere et al. is to use transient information of a modestly deformed drop relaxing back to a spherical shape in order to estimate the interfacial tension.

The problem of estimating interfacial tension from the

Present address of M. Tjahjadi: General Electric Corporate R&D, Schenectady, NY 12301.

growth of capillary instabilities along the surface of an otherwise stationary fluid thread can be traced back to the work of Rayleigh (1879) and Tomotika (1935). Similarly, because surfactants frequently modify substantially the interfacial tension, the growth of capillary instabilities on fluid jets can be used to measure the dynamic surface tension (Adamson, 1990; Ronay, 1978).

In this article, we describe an improved, though still approximate, procedure for determining the constant interfacial tension acting at the interface between two Newtonian fluids. The procedure utilizes *time-dependent experiments* which involve *time-dependent shapes* of relaxing drops. Curve-fit equations for the shape evolution are developed from numerical solutions of Stokes equations using boundary integral methods for similar model free-boundary problems. The result is a fast and accurate method for determining the interfacial tension of neutrally buoyant fluid-fluid systems. With suitable care and small Deborah number [$De < O(0.1)$; De measures the ratio of the fluid relaxation time to the flow time scale], the method used here can be applied to viscoelastic liquids. This method has previously been used by Tjahjadi et al. (1992, Table 1) who showed it to be in good agreement with interfacial tension estimates deduced from small deformation theory and linear stability theory. Finally, the method is compared to the published data by Carriere et al. (1989) and Elemans et al. (1990) and is shown to be in good agreement with their interfacial tension estimates.

Transient Shape Distortions and Measurement of Interfacial Tension

In this section we describe the typical experiments and numerical simulations for using transient drop deformation or the growth of capillary instabilities to determine the interfacial tension. A typical comparison of theory and experiment is presented.

Drop deformation and interfacial tension measurement

The "drop retraction" method (Carriere et al., 1989; Cohen and Carriere, 1989) and the "breaking thread" method (Elemans et al., 1990; Tomotika, 1935) are procedures for measuring the interfacial tension of very high-viscosity liquids. The experimental techniques, however, are in principle suitable for a wide range of fluid viscosities. In each of the methods, it is necessary to start with a deformed drop which is then allowed to relax. For example, the drop may be deformed into a cigar shape by a shear flow and then allowed to retract back to a sphere (Carriere et al., 1989) or as in the studies of Elemens et al. (1990), polymer threads, which are placed in an immiscible fluid matrix material, break owing to the growth of capillary instabilities as the temperature is increased and the polymer melts.

Carriere et al. deduce a value for the interfacial tension from a simplified, rather *ad hoc*, model of the relaxation dynamics of a drop. Elemans et al. used linear stability theory (Rayleigh, 1879) for a Newtonian thread in a quiescent fluid to estimate interfacial tension from time-dependent measurements of the amplitude of the surface distortion. An improvement of both of these methods requires detailed models for the interface shape as a function of time. We propose using efficiently tabulated results from a large number of numerical simulations that are able to capture the essential aspects of the time-dependent interface shape evolution. For ease of use and presentation, the numerical results have been curve-fit to simple polynomials in time with coefficients which are the function of the viscosity ratio between the two fluids.

Boundary integral calculations (Tanzosh et al., 1992; Pozrikidis, 1992) are well suited for studying free-boundary problems at low Reynolds numbers. The method has been used to study the deformation of a drop in an extensional flow (Rallison and Acrivos, 1978), the relaxation of modestly deformed drops (Stone and Leal, 1989), and the capillary instabilities of cylindrical threads (Tjahjadi et al., 1992). These studies offer details of the method.

The aspect ratio AR of the drop filament is defined as the ratio of the filament length $2L(t=0)$ to the filament mean diameter, $2a_0$, so that $AR = L(0)/a_0$ (see Figure 1). Such a definition is reasonable as long as at $t=0$ the radius a_0 along the filament is uniform and the ends are hemispherical, which closely approximates the thread shapes formed in the experiments of Carriere et al. The ratio of the drop viscosity, μ_i, to the suspending fluid viscosity, μ_e, is denoted $p = \mu_i/\mu_e$.

In all the experiments, the Reynolds numbers characterizing the interfacial-tension-driven relaxational motions must be small [$< O(10^{-1})$] and are defined by $Re = \rho\sigma r_0/\mu_e^2$ for the modestly deformed drop experiments (r_0 is the undeformed drop radius) and $Re = \rho\sigma a_0/\mu_e^2$ for the capillary breakup experiments.

Experiments and numerical simulations (Stone and Leal, 1989) indicate that two time-dependent deformation scenarios are possible: (i) moderately extended drops, $AR < AR_{crit}(p)$, retract back to a spherical shape without fragmentation; (ii) highly extended filaments, $AR \gg AR_{crit}(p)$, undergo fragmentation owing primarily to capillary instabilities.

Figure 2 shows a range of AR_{crit} computed for a range of viscosity ratios p via boundary integral techniques. Note that AR_{crit} is defined as the *smallest* aspect ratio of a filament to undergo the *first* breakup event. The breakup dynamics present a rich behavior as the aspect ratio is increased. A representative set of laboratory experiments is presented in Figure 3. Below AR_{crit}, the filament retracts to a spherical shape and breakup does not occur (Figure 3a). For AR at or slightly above AR_{crit}, the filament evolves into a dumbbell shape with two bulbous

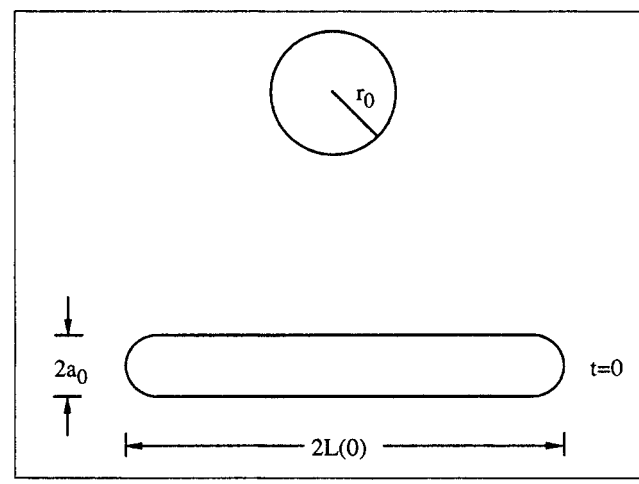

Figure 1. Initial condition for cylindrical filaments at $t=0$.

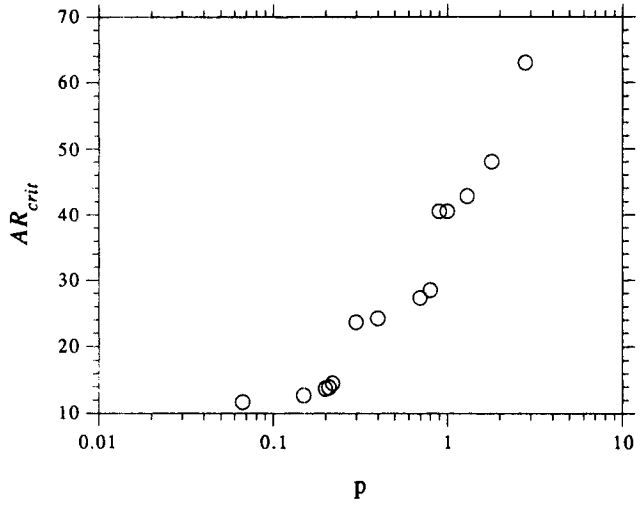

Figure 2. Critical aspect ratio of a fluid cylinder, AR_{crit}, for a range of viscosity ratios, p.

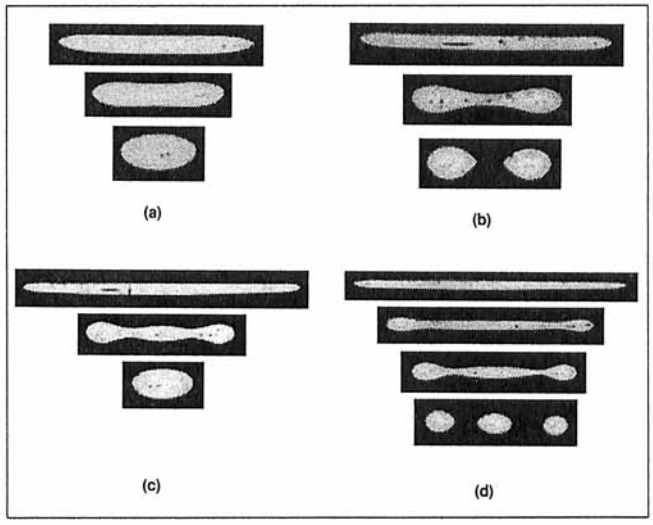

Figure 3. Experiment showing the dynamics of breakup or retraction as initial filament aspect ratio AR increases from (a) to (d); viscosity ratio $p = 0.067$.

ends. The first breakup occurs along the thin thread (or neck) and produces two droplets with a tiny satellite in-between (Figure 3b). As we increase the aspect ratio further, the thread evolution is such that the neck section fattens, while the ends relax in such a manner as to overcome the tendency to fragment and the filament retracts to a spherical shape (Figure 3c). As we further increase the aspect ratio, breakup occurs producing three large droplets with small satellites in-between (Figure 3d). The rather unusual recovery indicated by Figures 3b (fragmentation) and 3c (recovery to a spherical shape) has not been previously documented, though it is confined to a narrow range of aspect ratios. In this article, we only consider the case $AR < AR_{crit}$ in the "drop retraction" method.

Experiments

Before describing the two approximate methods for determining interfacial tension, the two types of experiments are described and the drop shapes are compared with numerical simulations.

Droplets are stretched in a Couette flow apparatus. The suspending fluid is transparent corn syrup 1632 (Corn Products, Englewood Cliffs, NJ). The drop fluid is a homogeneous mixture of oxidized castor oil (CasChem Inc., Bayonne, NJ), and 1-Bromonaphthalene (Aldrich Chemical), darkened by an organic dye (Oil Blue N, Aldrich Chemical). The viscosity ratio can be varied by changing the volume fraction of 1-Bromonaphthalene in the mixture. The experiment is started by injecting a drop below the surface of the bulk fluid. Drop deformation is generated by rotating the cylinders in opposite directions with a shear rate high enough to exceed the critical capillary number necessary for continuous drop extension. Once the desired length is achieved, the flow is stopped.

Experiments are recorded photographically using a camera connected to a stereomicroscope. The unperturbed radius of the filament is measured directly from the stereomicroscope; however, the dimensions of the filament during the evolution are measured from enlarged prints. The accuracy of the measurement is ± 5 μm. The time evolution is recorded by an intervalometer (Nikon MT2). Additional details on the experimental setup are provided by Tjahjadi et al. (1992).

In the first method, we consider the relaxation of a modestly deformed drop back to a spherical shape (Stone and Leal, 1989). Throughout this article, we use the term "modestly deformed" in a qualitative sense to indicate that the drop recovers a spherical shape when an external flow is removed. Photographs from a typical experiment and the corresponding numerical simulations at the same values of dimensionless time are presented in Figure 4.

In the second method, we consider the relaxation of a highly elongated drop where fragmentation, far from the ends, is driven by capillary instabilities (Tjahjadi et al., 1992). Once again, we present photographs from a typical experiment and

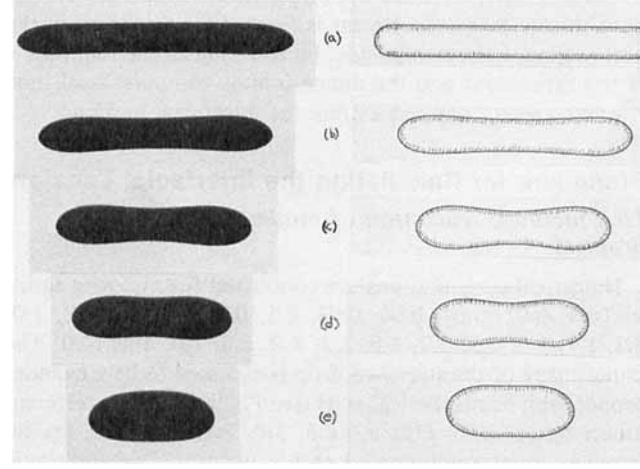

Figure 4. Experiment (left) and corresponding simulation (right) showing dynamics of relaxation of a cylindrical filament with $L(0)/a_0 = 8.9$ in otherwise quiescent fluid.

The unperturbed radius of the filament $a_0 = 0.074$ cm and the viscosity ratio $p = 0.067$. The viscosity of the bulk fluid is 290 $g \cdot cm^{-1} \cdot s^{-1}$. The dimensionless times, top to bottom, are $t = 0.0$, 5.4, 9.5, 14.7, and 18.1, respectively.

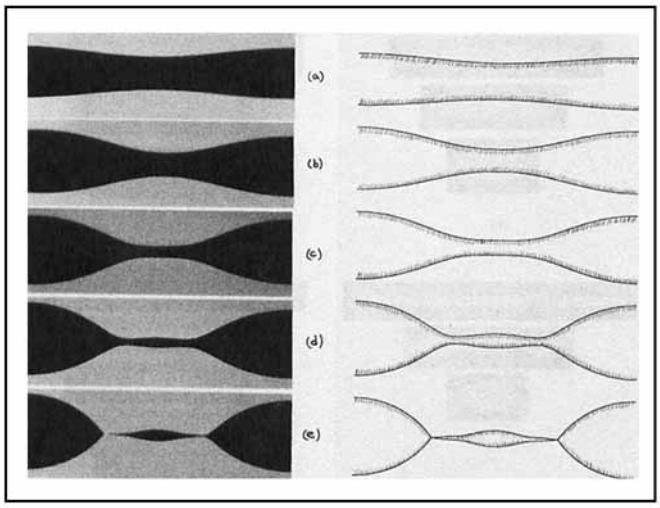

Figure 5. Experiment (left) and corresponding simulation (right) showing deformation of a segment of a highly stretched cylindrical filament, far from ends, in otherwise quiescent fluid.

The fluids are the same as in Figure 4. The unperturbed radius of the filament $a_0 = 0.04$ cm. The wave number for the segment shown is $x \approx 0.50$ ($x = 2\pi a_0/\lambda$, where λ is the wavelength). The dimensionless times, top to bottom, are $t = 0.0$, 7.4, 10.6, 12.7, and 14.4, respectively.

the corresponding numerical simulations in Figure 5. Initially, relatively small disturbances on the surface of the thread take the form of a sinusoidal wave of a single wavelength (this is precisely the initial condition chosen in our simulation). At later times, when the curvature gradient along the interface develops, the interfacial-tension-driven motion becomes highly nonlinear, and linear theory is no longer representative of the dynamics. However, boundary integral simulations successfully capture the rich physics of the *self-repeating* breakup dynamics around the trough part of the wave (Tjahjadi et al., 1992).

The characteristic time for the interfacial-tension-driven motions shown in the experiment is $t_c = a_0\mu_e/\sigma$. As shown in the next section, in both methods, by referring to the real time τ of the experiment and the dimensionless computational time t, where $t = \tau/t_c$, one can extract the interfacial tension.

Procedure for Calculating the Interfacial Tension

First method: relaxation of moderately extended droplets

Numerical computations are conducted for viscosity ratios $p = 0.01$, 0.02, 0.04, 0.06, 0.08, 0.1, 0.2, 0.4, 0.6, 0.8, 1.0, 1.3, 1.7, 2.0, 2.3, 2.7, 3.0, 3.3, 4.0, 5.0, 7.0, and 10.0. The initial shape of the stretched drop is assumed to be a cylinder capped with hemispherical ends (see Figure 1). Four different aspect ratios, $AR = L(0)/a_0 = 2.5$, 5.0, 7.5, and 10.0, are selected as initial conditions for each value of p. Two additional aspect ratios, $AR = 15.0$ and 20.0, are also selected for $p \geq 0.4$. The dynamics of drop retraction, in this case the dimensionless drop length $L(t)/r_0$, is curve-fit, using the method of least squares, to a polynomial as a function of time (99.9% accuracy):

$$L(t)/r_0 = \sum_{n=0}^{4} k_n(p)t^n. \tag{1}$$

The five coefficients, k_0–k_4, for all viscosity ratios and initial aspect ratios AR, are provided in Table 1 (note that on the lefthand side of Eq. 1 the undeformed drop radius r_0 is selected because it is easy to measure).

The calculation of the interfacial tension σ proceeds as follows:

1. Determine the viscosity ratio $p = \mu_i/\mu_e$.
2. Once a moderately elongated filament is attained and the external flow is stopped, record the filament's undeformed radius, a_0, measured at the filament's midpoint and half length, $L(0)$ (in cm) [note that $2L(0)$ is the total length of the filament]. The radius of the drop at rest is given by $r_0 \approx [0.5a_0^2(3L(0) - a_0)]^{1/3}$.
3. Record two images while the filament is retracting (such as Figures 4b and 4d) and record the time difference, $\Delta\tau$ (in s) and the corresponding drop half lengths $L(t)$s (in cm). For better accuracy, we recommend that $L(t)/r_0 > 1.5$ in both images.
4. Some linear interpolation is required to obtain the $L(t)/r_0$ profile which corresponds to the experiment. First, plot $L(t)/r_0$ (Eq. 1) with the coefficients provided in Table 1 corresponding to the closest viscosity ratio and initial aspect ratio. For example, for the experiment shown in Figure 4 ($p = 0.067$, $L(0)/a_0 = 8.9$), we plot $L(t)/r_0$ corresponding to $p = 0.06$ and 0.08 and initial aspect ratios $L(0)/a_0 = 7.5$ and 10.0 (see Figure 6). Then, interpolate to obtain curves that correspond to $p = 0.067$ and $L(0)/a_0 = 7.5$, and $p = 0.067$ and $L(0)/a_0 = 10.0$. From these two curves, interpolate again to obtain a curve that corresponds to $L(0)/a_0 = 8.9$ and $p = 0.067$ which is shown by the dashed line in Figure 6.
5. Plot two values of $L(t)/r_0$ obtained in step 3 on the dashed line obtained in step 4 (marked by "X" in Figure 6). Record the dimensionless time difference, Δt.
6. The interfacial tension is given by $\sigma = a_0\mu_e\Delta t/\Delta\tau$ (in $g \cdot s^{-2}$). The errors are estimated as follows: $a_0 \pm 0.5\%$, $\mu_e \pm 5\%$, $\Delta t \pm 1\%$, $\Delta\tau \pm 0.5\%$. Straightforward error analyses indicate that the error in σ is expected to be less than 10%.

Second method: breakup of highly extended fluid filaments

Again, numerical computations are conducted for viscosity ratios $p = 0.01$, 0.02, 0.04, 0.06, 0.08, 0.1, 0.2, 0.4, 0.6, 0.8, 1.0, 1.3, 1.7, 2.0, 2.3, 2.7, 3.0, 3.3, 4.0, 5.0, 7.0, and 10.0. The initial perturbation on the highly elongated fluid thread is assumed to be sinusoidal with amplitude, $A_{max} = A_{min} = 0.01\ a_0$, and wave number $x = x_{opt}$ (based on linear stability theory, there is an optimum wavenumber, $x_{opt} = 2\pi a_0/\lambda_{opt}$, which corresponds to the maximum rate of growth, see Figure 7). The evolution of the filament is recorded in terms of the maximum and minimum amplitudes, $A_{max}(t)$ and $A_{min}(t)$, of the initially sinusoidal disturbance. The dynamics of amplitudes growth, in this case the dimensionless maximum and minimum amplitudes, $A_{max}(t)/a_0$ and $A_{min}(t)/a_0$, are curve-fit, using the method of least squares, to a polynomial as a function of time (99.9% accuracy):

$$A_{max}(t)/a_0 = \sum_{n=0}^{3} k_n'(p)t^n, \tag{2}$$

$$A_{min}(t)/a_0 = \sum_{n=0}^{8} k_n''(p)t^n, \tag{3}$$

Table 1. Polynomial Coefficients of Eq. 1 for a Range of Viscosity Ratios p and Initial Aspect Ratios $L(0)/a_0$

p	$L(0)/a_0$	k_0	k_1	k_2	k_3	k_4
0.01	2.5	1.695	-1.687×10^{-1}	2.715×10^{-3}	2.214×10^{-3}	-1.474×10^{-4}
	5.0	2.619	-1.411×10^{-1}	-2.347×10^{-2}	3.299×10^{-3}	-1.057×10^{-4}
	7.5	3.393	-1.125×10^{-1}	-2.201×10^{-2}	1.893×10^{-3}	-4.032×10^{-5}
	10.0	4.102	-1.259×10^{-1}	-9.777×10^{-3}	5.663×10^{-4}	-6.824×10^{-6}
0.02	2.5	1.697	-1.775×10^{-1}	8.236×10^{-3}	1.093×10^{-3}	-8.107×10^{-5}
	5.0	2.620	-1.399×10^{-1}	-2.065×10^{-2}	2.817×10^{-3}	-8.605×10^{-5}
	7.5	3.392	-1.112×10^{-1}	-1.753×10^{-2}	1.408×10^{-3}	-2.747×10^{-5}
	10.0	4.124	-1.498×10^{-1}	1.155×10^{-3}	-5.550×10^{-5}	2.284×10^{-6}
0.04	2.5	1.691	-1.479×10^{-1}	-7.972×10^{-3}	4.047×10^{-3}	-2.542×10^{-4}
	5.0	2.618	-1.293×10^{-1}	-1.925×10^{-2}	2.446×10^{-3}	-7.055×10^{-5}
	7.5	3.388	-1.073×10^{-1}	-1.297×10^{-2}	9.490×10^{-4}	-1.638×10^{-5}
	10.0	4.126	-1.498×10^{-1}	1.108×10^{-3}	-5.142×10^{-5}	2.196×10^{-6}
0.06	2.5	1.695	-1.642×10^{-1}	4.397×10^{-3}	1.438×10^{-3}	-9.118×10^{-5}
	5.0	2.615	-1.208×10^{-1}	-1.801×10^{-2}	2.155×10^{-3}	-5.909×10^{-5}
	7.5	3.390	-1.077×10^{-1}	-9.642×10^{-3}	6.624×10^{-4}	-1.021×10^{-5}
	10.0	4.129	-1.498×10^{-1}	2.603×10^{-3}	-1.132×10^{-4}	2.596×10^{-6}
0.08	2.5	1.695	-1.583×10^{-1}	2.879×10^{-3}	1.566×10^{-3}	-9.476×10^{-5}
	5.0	2.614	-1.147×10^{-1}	-1.685×10^{-2}	1.924×10^{-3}	-5.059×10^{-5}
	7.5	3.390	-1.073×10^{-1}	-7.547×10^{-3}	4.926×10^{-4}	-6.827×10^{-6}
	10.0	4.133	-1.487×10^{-1}	3.379×10^{-3}	-1.410×10^{-4}	2.676×10^{-6}
0.1	2.5	1.692	-1.444×10^{-1}	-3.106×10^{-3}	2.485×10^{-3}	-1.415×10^{-4}
	5.0	2.612	-1.082×10^{-1}	-1.634×10^{-2}	1.788×10^{-3}	-4.563×10^{-5}
	7.5	3.395	-1.103×10^{-1}	-5.362×10^{-3}	3.325×10^{-4}	-3.748×10^{-6}
	10.0	4.133	-1.470×10^{-1}	3.730×10^{-3}	-1.519×10^{-4}	2.648×10^{-6}
0.2	2.5	1.692	-1.281×10^{-1}	-4.742×10^{-3}	2.253×10^{-3}	-1.172×10^{-4}
	5.0	2.610	-9.623×10^{-2}	-1.183×10^{-2}	1.133×10^{-3}	-2.500×10^{-5}
	7.5	3.398	-1.061×10^{-1}	-1.982×10^{-3}	1.073×10^{-4}	-3.537×10^{-7}
	10.0	4.131	-1.307×10^{-1}	3.244×10^{-3}	-1.128×10^{-4}	1.617×10^{-6}
0.4	2.5	1.694	-1.149×10^{-1}	-1.839×10^{-3}	1.216×10^{-3}	-5.484×10^{-5}
	5.0	2.609	-8.606×10^{-2}	-7.422×10^{-3}	6.166×10^{-4}	-1.139×10^{-5}
	7.5	3.398	-9.502×10^{-2}	-8.126×10^{-4}	4.430×10^{-5}	3.082×10^{-8}
	10.0	4.126	-1.118×10^{-1}	2.360×10^{-3}	-6.978×10^{-5}	8.561×10^{-7}
	15.0	5.401	-1.030×10^{-1}	1.565×10^{-3}	-2.071×10^{-5}	1.103×10^{-7}
	20.0	6.511	-8.911×10^{-2}	9.753×10^{-4}	-8.479×10^{-6}	2.800×10^{-8}
0.6	2.5	1.692	-1.008×10^{-1}	-2.080×10^{-3}	9.470×10^{-4}	-3.834×10^{-5}
	5.0	2.610	-8.261×10^{-2}	-4.870×10^{-3}	3.776×10^{-4}	-6.071×10^{-6}
	7.5	3.400	-9.099×10^{-2}	-3.009×10^{-5}	7.319×10^{-6}	3.514×10^{-7}
	10.0	4.118	-9.839×10^{-2}	1.591×10^{-3}	-4.082×10^{-5}	4.712×10^{-7}
	15.0	5.390	-9.609×10^{-2}	1.121×10^{-3}	-1.313×10^{-5}	6.451×10^{-8}
	20.0	6.514	-8.177×10^{-2}	8.097×10^{-4}	-6.682×10^{-6}	2.161×10^{-8}
0.8	2.5	1.692	-9.384×10^{-2}	-9.203×10^{-4}	6.258×10^{-4}	-2.331×10^{-5}
	5.0	2.608	-7.734×10^{-2}	-3.970×10^{-3}	2.934×10^{-4}	-4.478×10^{-6}
	7.5	3.393	-8.043×10^{-2}	-6.645×10^{-4}	3.612×10^{-5}	-1.626×10^{-7}
	10.0	4.110	-8.828×10^{-2}	1.017×10^{-3}	-2.195×10^{-5}	2.547×10^{-7}
	15.0	5.392	-8.689×10^{-2}	1.105×10^{-3}	-1.368×10^{-5}	6.919×10^{-8}
	20.0	6.507	-7.553×10^{-2}	6.577×10^{-4}	-4.996×10^{-6}	1.534×10^{-8}
1.0	2.5	1.707	-8.392×10^{-2}	-1.638×10^{-3}	5.586×10^{-4}	-1.861×10^{-5}
	5.0	2.628	-7.634×10^{-2}	-2.695×10^{-3}	1.956×10^{-4}	-2.670×10^{-6}
	7.5	3.414	-7.852×10^{-2}	-2.978×10^{-4}	2.062×10^{-5}	-3.126×10^{-8}
	10.0	4.128	-8.310×10^{-2}	8.248×10^{-4}	-1.561×10^{-5}	1.752×10^{-7}
	15.0	5.396	-8.070×10^{-2}	9.187×10^{-4}	-1.079×10^{-5}	5.295×10^{-8}
	20.0	6.517	-7.202×10^{-2}	6.086×10^{-4}	-4.619×10^{-6}	1.420×10^{-8}
1.3	2.5	1.691	-8.150×10^{-2}	6.488×10^{-4}	2.364×10^{-4}	-7.581×10^{-6}
	5.0	2.610	-7.255×10^{-2}	-2.114×10^{-3}	1.542×10^{-4}	-2.053×10^{-6}
	7.5	3.393	-7.187×10^{-2}	-5.390×10^{-4}	2.952×10^{-5}	-1.790×10^{-7}
	10.0	4.107	-7.611×10^{-2}	5.114×10^{-4}	-7.059×10^{-6}	9.134×10^{-8}
	15.0	5.388	-7.598×10^{-2}	7.699×10^{-4}	-8.470×10^{-6}	4.052×10^{-8}
	20.0	6.508	-6.872×10^{-2}	5.436×10^{-4}	-3.990×10^{-6}	1.207×10^{-8}
1.7	2.5	1.692	-7.440×10^{-2}	1.078×10^{-3}	1.225×10^{-4}	-3.720×10^{-6}
	5.0	2.613	-7.058×10^{-2}	-1.229×10^{-3}	9.762×10^{-5}	-1.196×10^{-6}
	7.5	3.396	-6.881×10^{-2}	-3.435×10^{-4}	2.175×10^{-5}	-1.256×10^{-7}
	10.0	4.103	-6.952×10^{-2}	2.601×10^{-4}	-7.704×10^{-7}	3.207×10^{-8}
	15.0	5.383	-7.035×10^{-2}	6.099×10^{-4}	-6.215×10^{-6}	2.924×10^{-8}
	20.0	6.503	-6.391×10^{-2}	4.390×10^{-4}	-2.987×10^{-6}	8.785×10^{-9}

(*continued*)

Table 1. Polynomial Coefficients of Eq. 1 for a Range of Viscosity Ratios p and Initial Aspect Ratios $L(0)/a_0$ (continued)

p	$L(0)/a_0$	k_0	k_1	k_2	k_3	k_4
2.0	2.5	1.692	-7.080×10^{-2}	1.410×10^{-3}	6.226×10^{-5}	-1.971×10^{-6}
	5.0	2.613	-6.835×10^{-2}	-8.969×10^{-4}	7.599×10^{-5}	-8.932×10^{-7}
	7.5	3.394	-6.500×10^{-2}	-4.302×10^{-4}	2.384×10^{-5}	-1.595×10^{-7}
	10.0	4.103	-6.649×10^{-2}	1.881×10^{-4}	8.339×10^{-7}	1.581×10^{-8}
	15.0	5.378	-6.646×10^{-2}	4.942×10^{-4}	-4.615×10^{-6}	2.161×10^{-8}
	20.0	6.502	-6.142×10^{-2}	3.916×10^{-4}	-2.572×10^{-6}	7.509×10^{-9}
2.3	2.5	1.690	-5.355×10^{-2}	8.128×10^{-4}	3.012×10^{-5}	-7.595×10^{-7}
	5.0	2.620	-6.384×10^{-2}	1.820×10^{-4}	1.906×10^{-5}	-1.977×10^{-7}
	7.5	3.397	-5.870×10^{-2}	-1.474×10^{-4}	1.301×10^{-5}	-8.320×10^{-8}
	10.0	4.098	-5.652×10^{-2}	-2.311×10^{-5}	4.786×10^{-6}	-1.952×10^{-8}
	15.0	5.358	-5.464×10^{-2}	1.844×10^{-4}	-6.970×10^{-7}	4.230×10^{-9}
	20.0	6.471	-5.018×10^{-2}	1.619×10^{-4}	-6.143×10^{-7}	1.869×10^{-9}
2.7	2.5	1.690	-5.870×10^{-2}	7.104×10^{-4}	6.183×10^{-5}	-1.568×10^{-6}
	5.0	2.616	-6.512×10^{-2}	-2.423×10^{-4}	3.896×10^{-5}	-4.185×10^{-7}
	7.5	3.394	-6.067×10^{-2}	-2.962×10^{-4}	1.809×10^{-5}	-1.200×10^{-7}
	10.0	4.095	-5.870×10^{-2}	-5.658×10^{-5}	5.764×10^{-6}	-2.332×10^{-8}
	15.0	5.359	-5.799×10^{-2}	2.530×10^{-4}	-1.495×10^{-6}	7.715×10^{-9}
	20.0	6.489	-5.523×10^{-2}	2.658×10^{-4}	-1.473×10^{-6}	4.230×10^{-9}
3.0	2.5	1.691	-5.707×10^{-2}	9.944×10^{-4}	2.934×10^{-5}	-8.107×10^{-7}
	5.0	2.617	-6.361×10^{-2}	-1.015×10^{-5}	3.095×10^{-5}	-3.250×10^{-7}
	7.5	3.396	-5.978×10^{-2}	-2.054×10^{-4}	1.506×10^{-5}	-9.763×10^{-8}
	10.0	4.095	-5.712×10^{-2}	-6.467×10^{-5}	5.736×10^{-6}	-2.424×10^{-8}
	15.0	5.360	-5.666×10^{-2}	2.344×10^{-4}	-1.305×10^{-6}	6.808×10^{-9}
	20.0	6.506	-5.520×10^{-2}	2.740×10^{-4}	-1.546×10^{-6}	4.392×10^{-9}
3.3	2.5	1.690	-5.355×10^{-2}	8.128×10^{-4}	3.012×10^{-5}	-7.595×10^{-7}
	5.0	2.620	-6.384×10^{-2}	1.820×10^{-4}	1.906×10^{-5}	-1.977×10^{-7}
	7.5	3.397	-5.870×10^{-2}	-1.474×10^{-4}	1.301×10^{-5}	-8.320×10^{-8}
	10.0	4.098	-5.652×10^{-2}	-2.311×10^{-5}	4.786×10^{-6}	-1.952×10^{-8}
	15.0	5.358	-5.464×10^{-2}	1.844×10^{-4}	-6.970×10^{-7}	4.230×10^{-9}
	20.0	6.471	-5.018×10^{-2}	1.619×10^{-4}	-6.143×10^{-7}	1.869×10^{-9}
4.0	2.5	1.690	-4.834×10^{-2}	7.773×10^{-4}	1.489×10^{-5}	-3.863×10^{-7}
	5.0	2.619	-5.921×10^{-2}	2.171×10^{-4}	1.357×10^{-5}	1.358×10^{-7}
	7.5	3.399	-5.665×10^{-2}	-2.648×10^{-5}	9.037×10^{-6}	-5.607×10^{-8}
	10.0	4.095	-5.309×10^{-2}	-5.703×10^{-5}	5.004×10^{-6}	-2.189×10^{-8}
	15.0	5.340	-4.875×10^{-2}	3.409×10^{-5}	9.790×10^{-7}	-2.145×10^{-9}
	20.0	6.477	-4.837×10^{-2}	1.445×10^{-4}	-5.116×10^{-7}	1.582×10^{-9}
5.0	2.5	1.691	-4.336×10^{-2}	8.091×10^{-4}	3.607×10^{-8}	-9.198×10^{-8}
	5.0	2.623	-5.649×10^{-2}	4.410×10^{-4}	3.659×10^{-6}	-4.420×10^{-8}
	7.5	3.407	-5.535×10^{-2}	1.577×10^{-4}	4.123×10^{-6}	-2.554×10^{-8}
	10.0	4.101	-5.145×10^{-2}	2.475×10^{-5}	3.258×10^{-6}	-1.392×10^{-8}
	15.0	5.336	-4.526×10^{-2}	-9.266×10^{-6}	1.312×10^{-6}	-3.358×10^{-9}
	20.0	6.448	-4.233×10^{-2}	3.602×10^{-5}	2.876×10^{-7}	-3.995×10^{-10}
7.0	2.5	1.691	-3.465×10^{-2}	5.652×10^{-4}	-1.822×10^{-6}	-1.961×10^{-8}
	5.0	2.623	-4.879×10^{-2}	4.276×10^{-4}	-4.668×10^{-9}	-1.025×10^{-8}
	7.5	3.408	-4.997×10^{-2}	2.194×10^{-4}	1.431×10^{-6}	-9.806×10^{-9}
	10.0	4.112	-4.867×10^{-2}	1.268×10^{-4}	1.211×10^{-6}	-5.388×10^{-9}
	15.0	5.348	-4.276×10^{-2}	1.854×10^{-5}	8.813×10^{-7}	-2.224×10^{-9}
	20.0	6.455	-3.916×10^{-2}	1.885×10^{-5}	3.473×10^{-7}	-5.722×10^{-10}
10.0	2.5	1.690	-2.674×10^{-2}	3.644×10^{-4}	-1.655×10^{-6}	-7.946×10^{-10}
	5.0	2.622	-4.049×10^{-2}	3.499×10^{-4}	-1.031×10^{-6}	-1.050×10^{-11}
	7.5	3.415	-4.470×10^{-2}	2.690×10^{-4}	-4.191×10^{-7}	-6.303×10^{-10}
	10.0	4.125	-4.511×10^{-2}	1.905×10^{-4}	-3.918×10^{-8}	-8.695×10^{-10}
	15.0	5.365	-4.012×10^{-2}	5.967×10^{-5}	3.615×10^{-7}	-9.412×10^{-10}
	20.0	6.488	-3.738×10^{-2}	4.099×10^{-5}	1.702×10^{-7}	-3.120×10^{-10}

where the coefficients, k_n' in Eq. 2 and k_n'' in Eq. 3, for all viscosity ratios are provided in Table 2.

Initially, the relatively small disturbances on the surface of the thread are sinusoidal (see Figures 5a-5b) with amplitudes A_{max} and A_{min} which grow at the same rate; the growth rate is the largest when $x=x_{opt}$. As the curvature develops, the interfacial-tension-driven motion becomes highly nonlinear and produces a slender tube around the trough part of the wave (Figure 5c); the ends of the slender tube are connected to the large mother drops originating from the crest parts of the wave. Due to the nonlinear dynamical evolution of the highly deformed shapes coupled with the prerequisite of 99.9% accuracy, a relatively large number of polynomial coefficients are required in Eq. 3. It should be pointed out that to the extent that it is impossible to start with a filament with a perfectly uniform radius and symmetric initial perturbation, the first fragmentation of the drop almost never occurs simultaneously (Figure 5e). However, to calculate the interfacial tension, a

Table 2. Polynomial Coefficients of Eqs. 2 and 3 for a Range of Viscosity Ratios p^*

p	Eq. 2	k_0'	k_1'	k_2'	k_3'	
		k_4'	k_5'			
(x)	Eq. 3	k_0''	k_1''	k_2''	k_3''	
		k_4''	k_5''	k_6''	k_7''	k_8''
0.01	Eq. 2	1.448×10^{-2}	1.329×10^{-3}	3.346×10^{-4}	9.008×10^{-5}	
(0.42)	Eq. 3	8.787×10^{-3}	1.069×10^{-2}	-1.432×10^{-2}	8.142×10^{-3}	
		-2.184×10^{-3}	3.169×10^{-4}	-2.520×10^{-5}	1.035×10^{-6}	-1.709×10^{-8}
0.02	Eq. 2	1.165×10^{-2}	3.392×10^{-3}	-3.032×10^{-4}	7.125×10^{-5}	
(0.47)	Eq. 3	9.672×10^{-3}	4.677×10^{-2}	-4.410×10^{-3}	2.410×10^{-3}	
		-5.844×10^{-4}	7.569×10^{-5}	-5.304×10^{-6}	1.905×10^{-7}	-2.732×10^{-9}
0.04	Eq. 2	9.605×10^{-3}	3.556×10^{-3}	-3.374×10^{-4}	3.790×10^{-5}	
(0.52)	Eq. 3	1.492×10^{-2}	-1.465×10^{-2}	1.079×10^{-2}	-2.775×10^{-3}	
		3.545×10^{-4}	-2.371×10^{-5}	8.282×10^{-7}	-1.336×10^{-8}	6.607×10^{-11}
0.06	Eq. 2	8.299×10^{-3}	3.572×10^{-2}	-3.043×10^{-4}	2.420×10^{-5}	
(0.54)	Eq. 3	1.638×10^{-2}	-1.581×10^{-2}	9.692×10^{-3}	-2.146×10^{-3}	
		2.382×10^{-4}	-1.412×10^{-5}	4.515×10^{-7}	-7.156×10^{-9}	4.254×10^{-11}
0.08	Eq. 2	5.967×10^{-3}	4.058×10^{-3}	-3.120×10^{-4}	1.784×10^{-5}	
(0.56)	Eq. 3	1.650×10^{-2}	-1.475×10^{-2}	8.056×10^{-3}	-1.590×10^{-3}	
		1.571×10^{-4}	-8.324×10^{-6}	2.391×10^{-7}	-3.444×10^{-9}	1.903×10^{-11}
0.1	Eq. 2	4.610×10^{-3}	4.142×10^{-3}	-2.895×10^{-4}	1.362×10^{-5}	
(0.57)	Eq. 3	1.609×10^{-2}	-1.282×10^{-2}	6.379×10^{-3}	-1.138×10^{-3}	
		1.017×10^{-4}	-4.872×10^{-6}	1.268×10^{-7}	-1.660×10^{-9}	8.391×10^{-12}
0.2	Eq. 2	-3.243×10^{-4}	4.164×10^{-3}	-2.074×10^{-4}	5.629×10^{-6}	
(0.59)	Eq. 3	1.496×10^{-2}	-6.623×10^{-3}	2.355×10^{-3}	-2.921×10^{-4}	
		1.825×10^{-5}	-6.089×10^{-7}	1.097×10^{-8}	-9.809×10^{-11}	3.296×10^{-13}
0.4	Eq. 2	-1.925×10^{-3}	3.340×10^{-3}	-1.215×10^{-4}	2.209×10^{-6}	
(0.59)	Eq. 3	1.604×10^{-2}	-6.420×10^{-3}	1.622×10^{-3}	-1.473×10^{-4}	
		6.726×10^{-6}	-1.656×10^{-7}	2.234×10^{-9}	-1.536×10^{-11}	4.164×10^{-14}
0.6	Eq. 2	-2.127×10^{-3}	2.806×10^{-3}	-8.510×10^{-5}	1.275×10^{-6}	
(0.58)	Eq. 3	1.4823×10^{-2}	-3.949×10^{-3}	8.412×10^{-4}	-6.270×10^{-5}	
		2.363×10^{-6}	-4.799×10^{-8}	5.332×10^{-10}	-3.007×10^{-12}	6.649×10^{-15}
0.8	Eq. 2	-1.681×10^{-3}	2.435×10^{-3}	-6.532×10^{-5}	8.622×10^{-7}	
(0.57)	Eq. 3	1.437×10^{-2}	-3.343×10^{-3}	6.341×10^{-4}	-4.157×10^{-5}	
		1.374×10^{-6}	-2.445×10^{-8}	2.381×10^{-10}	-1.178×10^{-12}	2.288×10^{-15}
1.0	Eq. 2	-6.436×10^{-4}	2.105×10^{-3}	-5.160×10^{-5}	6.283×10^{-7}	
(0.56)	Eq. 3	1.357×10^{-2}	-2.584×10^{-3}	4.568×10^{-4}	-2.713×10^{-5}	
		8.127×10^{-7}	-1.309×10^{-8}	1.153×10^{-10}	-5.156×10^{-13}	9.050×10^{-16}
1.3	Eq. 2	2.081×10^{-3}	1.603×10^{-3}	-3.582×10^{-5}	4.181×10^{-7}	
(0.55)	Eq. 3	1.474×10^{-2}	-2.975×10^{-3}	4.460×10^{-4}	-2.340×10^{-5}	
		6.190×10^{-7}	-8.836×10^{-9}	6.925×10^{-11}	-2.773×10^{-13}	4.395×10^{-16}
1.7	Eq. 2	4.204×10^{-3}	1.247×10^{-3}	-2.526×10^{-5}	2.754×10^{-7}	
(0.54)	Eq. 3	1.440×10^{-2}	-2.648×10^{-3}	3.541×10^{-4}	-1.640×10^{-5}	
		3.811×10^{-7}	-4.775×10^{-9}	3.284×10^{-11}	-1.156×10^{-13}	1.612×10^{-16}
2.0	Eq. 2	1.092×10^{-2}	6.193×10^{-4}	-1.360×10^{-5}	1.881×10^{-7}	
(0.52)	Eq. 3	1.426×10^{-2}	-2.294×10^{-3}	2.836×10^{-4}	-1.211×10^{-5}	
		2.603×10^{-7}	-3.022×10^{-9}	1.929×10^{-11}	-6.305×10^{-14}	8.188×10^{-17}
2.3	Eq. 2	1.215×10^{-2}	4.905×10^{-4}	-1.068×10^{-5}	1.489×10^{-7}	
(0.52)	Eq. 3	1.448×10^{-2}	-2.200×10^{-3}	2.513×10^{-4}	-9.973×10^{-6}	
		1.994×10^{-7}	-2.153×10^{-9}	1.279×10^{-11}	-3.891×10^{-14}	4.704×10^{-17}
2.7	Eq. 2	1.325×10^{-2}	3.767×10^{-4}	-8.028×10^{-6}	1.127×10^{-7}	
(0.51)	Eq. 3	1.391×10^{-2}	-1.668×10^{-3}	1.778×10^{-4}	-6.449×10^{-6}	
		1.185×10^{-7}	-1.175×10^{-9}	6.412×10^{-12}	-1.790×10^{-14}	1.980×10^{-17}
3.0	Eq. 2	2.045×10^{-2}	-8.488×10^{-5}	-2.050×10^{-6}	8.050×10^{-8}	
(0.50)	Eq. 3	1.428×10^{-2}	-1.717×10^{-3}	1.705×10^{-4}	-5.842×10^{-16}	
		1.013×10^{-7}	-9.496×10^{-10}	4.901×10^{-12}	-1.296×10^{-14}	1.363×10^{-17}
3.3	Eq. 2	1.518×10^{-2}	2.155×10^{-4}	-4.945×10^{-6}	7.669×10^{-8}	
(0.50)	Eq. 3	1.364×10^{-2}	-1.377×10^{-3}	1.291×10^{-4}	-4.189×10^{-6}	
		6.908×10^{-8}	-6.151×10^{-10}	3.014×10^{-12}	-7.553×10^{-15}	7.499×10^{-18}
4.0	Eq. 2	2.669×10^{-2}	-3.936×10^{-4}	1.737×10^{-6}	4.140×10^{-8}	
(0.48)	Eq. 3	1.319×10^{-2}	-1.044×10^{-3}	9.236×10^{-5}	-2.681×10^{-6}	
		3.966×10^{-8}	-3.167×10^{-10}	1.392×10^{-12}	-3.130×10^{-15}	2.789×10^{-18}
5.0	Eq. 2	2.651×10^{-2}	-1.878×10^{-3}	5.411×10^{-5}	-5.012×10^{-7}	
(0.46)		2.024×10^{-9}	-2.626×10^{-12}			
	Eq. 3	1.223×10^{-2}	-6.116×10^{-4}	5.180×10^{-5}	-1.329×10^{-6}	
		1.747×10^{-8}	-1.234×10^{-10}	4.793×10^{-13}	-9.499×10^{-16}	7.432×10^{-19}
7.0	Eq. 2	2.702×10^{-2}	-1.524×10^{-3}	3.518×10^{-5}	-2.622×10^{-7}	
(0.44)		8.548×10^{-10}	-8.946×10^{-13}			
	Eq. 3	1.141×10^{-2}	-2.697×10^{-4}	2.252×10^{-5}	-4.743×10^{-7}	
		5.191×10^{-9}	-3.030×10^{-11}	9.693×10^{-14}	-1.573×10^{-16}	1.002×10^{-19}
10.0	Eq. 2	2.381×10^{-2}	-9.637×10^{-4}	1.807×10^{-5}	-1.063×10^{-7}	
(0.41)		2.764×10^{-10}	-2.270×10^{-13}			
	Eq. 3	9.108×10^{-3}	1.945×10^{-4}	-1.254×10^{-6}	-2.116×10^{-9}	
		2.528×10^{-10}	-1.915×10^{-12}	6.332×10^{-15}	-9.443×10^{-18}	5.141×10^{-21}

*Note that for $p\leq4.0$, $k_4'=k_5'=0$.

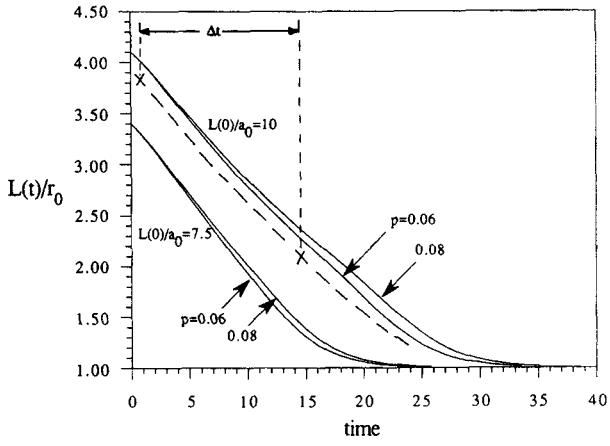

Figure 6. Time evolution of $L(t)/r_0$, obtained from Table 1, corresponding to $L(0)/a_0 = 7.5$ and 10.0 and $p = 0.06$ and 0.08. The dashed curve, obtained by interpolation, corresponds to $L(0)/a_0 = 8.9$ and $p = 0.067$.

radius variation of less than 10% for a wavelength interval along the axis is acceptable.

The calculation proceeds as follows (we determine two values of interfacial tension σ, one from A_{max} and the other from A_{min}):

1. Determine the viscosity ratio $p = \mu_i/\mu_e$.
2. Once a highly elongated filament is attained and the external flow is stopped, record the undeformed radius of the filament, a_0 (in cm).
3. Focus on a particular segment of the filament far away from the ends. Once a visible disturbance is observed, verify that the wave number $x \approx x_{opt} \pm 0.05$. If this criterion is not satisfied, repeat the experiment.
4. Record two images while the amplitude continues to grow (Figures 5b and 5d) and record the time difference, $\Delta\tau$ (in s). Measure A_{max} and A_{min} (in cm) and divide by a_0. For improved accuracy, we recommend A_{max}/a_0 or A_{min}/a_0 be greater than 0.2 in the first image and greater than 0.5 in the second image.
5. Plot A_{max}/a_0 and A_{min}/a_0 (Eqs. 2 and 3) with coefficients provided in Table 2 corresponding to the closest viscosity ratio(s). For example, for the experiment in Figure 5 ($p = 0.067$), plot A_{max}/a_0 and A_{min}/a_0 for $p = 0.06$ and 0.08 as in Figures 8a and 8b. Then, linearly interpolate for both A_{max}/a_0 and A_{min}/a_0 between the curves $p = 0.06$ and 0.08 as required to obtain profiles that approximately correspond to $p = 0.067$ (this interpolation is shown by the dashed lines in Figures 8a and 8b).
6. Plot the values of A_{max}/a_0 and A_{min}/a_0 in step 4 on the dashed lines that correspond to A_{max}/a_0 and A_{min}/a_0, respectively (marked by "X" in Figures 8a and 8b). Record the dimensionless time difference, Δt, and as a check on the consistency of this technique, we note that the values of Δt obtained from Figures 8a and b should be about the same.
7. The interfacial tension is given by $\sigma = a_0\mu_e\Delta t/\Delta\tau$ (in $g \cdot s^{-2}$). The errors are estimated as follows: $a_0 \pm 0.5\%$, $\mu_e \pm 5\%$, $\Delta t \pm 1\%$, $\Delta\tau \pm 0.5\%$. The error in σ is less than 10%.

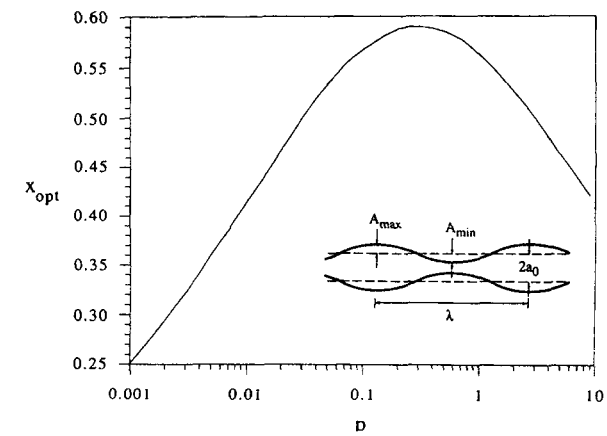

Figure 7. Optimum wave number, x_{opt}, as a function of viscosity ratio p.

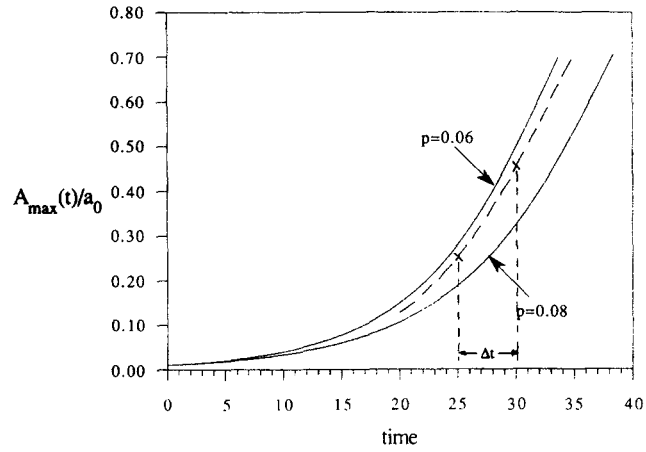

Figure 8a. Time evolution of $A_{max}(t)/a_0$, obtained from Table 2, corresponding to $p = 0.06$ and 0.08.

The dashed curve, obtained by interpolation, corresponds to $p = 0.067$.

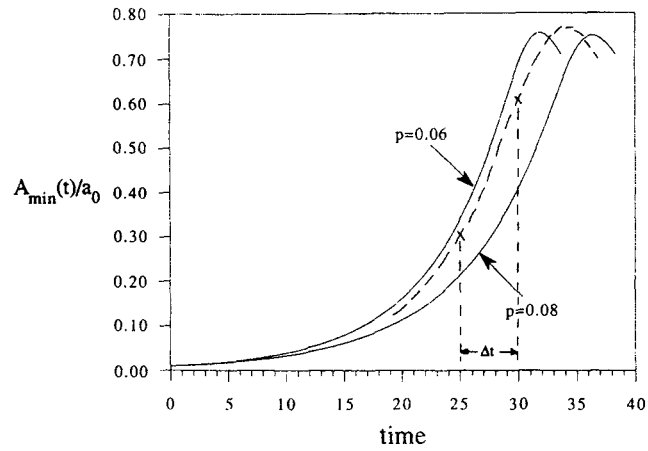

Figure 8b. Time evolution of $A_{min}(t)/a_0$, obtained from Table 2, corresponding to $p = 0.06$ and 0.08.

The dashed curve, obtained by interpolation, corresponds to $p = 0.067$.

Comparison with other techniques

In this section, we compare the two methods described above with published data by Carriere et al. (1989) and Elemans et al. (1990).

Table 3. Experimental Data of Fiber Retraction*

No.	μ_e ($g \cdot cm^{-1} \cdot s^{-1}$)	p	a_0 (cm)	$L(0)/a_0$	$\Delta\tau$ (s)	Δt	σ ($g \cdot s^{-2}$) Method 1	σ ($g \cdot s^{-2}$) Carriere et al.
5	20,000	0.1	0.017	2.5	2,520	9.4	1.27	1.40
10	20,000	0.1	0.012	5.6	2,940	17.0	1.39	1.60

*Extracted from Table III of Carriere et al. (1989)

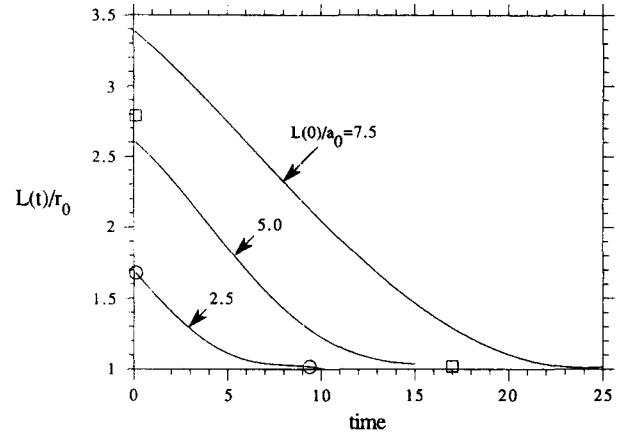

Figure 9a. Time evolution of $L(t)/r_0$, obtained from Table 1, corresponding to $L(0)/a_0 = 2.5$, 5.0, and 7.5 and $p = 0.1$.

○, experiment no. 5 ($p = 0.1$ and $L(0)/a_0 = 2.5$); □, experiment no. 10 ($p = 0.1$ and $L(0)/a_0 = 5.6$) of Table III from Carriere et al. (1989).

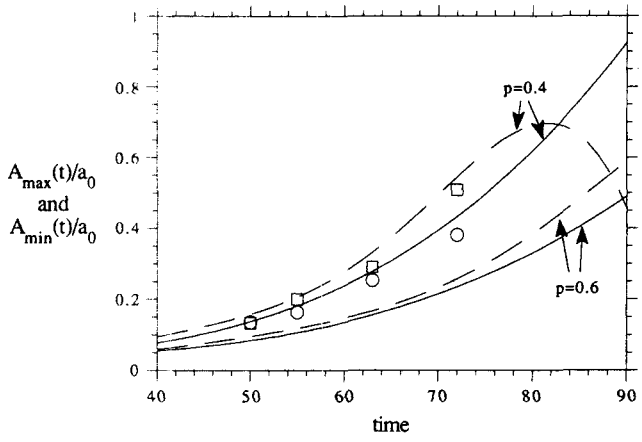

Figure 9b. Time evolution of $A_{max}(t)/a_0$ (—) and $A_{min}(t)/a_0$ (· · ·), obtained from Table 2, corresponding to $p = 0.4$ and 0.6.

Data are obtained using an image analyzer on Figure 1 from Elemans et al. (1990); ○, □, data for $A_{max}(t)/a_0$ and $A_{min}(t)/a_0$, respectively, and $p = 0.425$.

We first consider the raw data from fiber retraction experiments which are reported in Table III of Carriere et al. (1989). Specifically, we examine their experiments nos. 5 and 10; relevant data are given in Table 3.

The only information we require to estimate the interfacial tension is the dimensionless time Δt of the retraction experiment. This time is deduced from Figure 9a which is generated using the procedure described earlier. In all cases, the curves asymptotically approach the value $L(t)/r_0 = 1$ which corresponds to a spherical drop. Waiting for the drop to reach a spherical shape may introduce significant error to the interfacial tension estimate simply because a criterion must be given for determining when the drop has obtained a "spherical shape." For example, in Figure 9a it takes several units of dimensionless time for a drop to retract from $L(t)/r_0 = 1.1$ to 1.01. Choosing $L(t)/r_0 = 1.02$, so that the drop is within 2% of the spherical shape, our method provides values of σ within 12% of Carriere et al. (see Table 3).

Second, we estimate interfacial tension based on the thread breaking experimental data presented in Figure 1 of Elemans et al. (1990). The fiber dimensions obtained by analyzing the photographs using an image analyzer are given in Table 4. Again, we only need to determine the dimensionless time Δt between two photos as they are plotted in Figure 9b which is based on the procedure described earlier. The photos at $t = 15$ s and 45 s are used, as the filament has deformed sufficiently to minimize measurement error. The measured value of the wave amplitude is prone to considerable error when the amplitude is small [$A_{max}(t)/a_0 < 0.2$]. Our method produces a value within 20% of Elemans et al.

Conclusion

We have presented ready-to-use equations, cast as polynomials, to estimate fluid-fluid interfacial tension using two techniques: relaxation of moderately extended droplets and breakup of highly extended fluid filaments. The polynomial coefficients are obtained from boundary integral calculations which have been shown to simulate even the fine details of experiments and thus can be used to extract an excellent approximation to the interfacial tension. The two procedures offer improvement over earlier methods which were either *ad hoc* in their treatment of the fluid dynamics or restricted to the regime of linear stability theory.

Table 4. Experimental Data of Thread Breakup*

Time (s)	$A_{max}(t)/a_0$	$A_{min}(t)/a_0$	$p = 0.425$, $\mu_e = 10{,}000$ $g \cdot cm^{-1} \cdot s^{-1}$,
0	0.136	0.133	$a_0 = 0.00275$ cm
15	0.164	0.200	$\Delta t = 72 - 55$ (from Figure 9b) and $\Delta\tau = 45$ s − 15 s
30	0.254	0.291	σ (Method 2) = 15.6 $g \cdot s^{-2}$
45	0.382	0.509	σ (Elemans et al.) = 20.0 $g \cdot s^{-2}$

*Adapted from Figure 1 of Elemans et al. (1990)

Acknowledgment

This research has been supported by the Department of Energy, Office of Basic Energy Sciences. HAS was supported by an NSF-PYI Award (CTS-8957043).

Notation

A_{max} = amplitude of perturbation at the crest, cm (see inset Figure 7)
A_{min} = amplitude of perturbation at the trough, cm (see inset Figure 7)
AR = aspect ratio of filament, $AR = L(0)/a_0$
AR_{crit} = critical aspect ratio
a_0 = radius of filament at $t = 0$, cm
k, k', k'' = polynomial coefficients (see Eqs. 1, 2 and 3)
$L(t)$ = half length of filament at time t
p = viscosity ratio, $p = \mu_i/\mu_e$
r_0 = undeformed radius of the drop, cm
t = time, dimensionless, $t = \tau/t_c$
t_c = characteristic time of experiment, $t_c = a_0\mu_e/\sigma$
x = wave number, $x = 2\pi a_0/\lambda$
x_{opt} = optimum wave number

Greek letters

λ = wavelength, cm
σ = interfacial tension, $g \cdot s^{-2}$
τ = time, s
ρ = density
μ_e = viscosity of external (suspending) fluid, $g \cdot cm^{-1} \cdot s^{-1}$
μ_i = viscosity of internal (drop) fluid, $g \cdot cm^{-1} \cdot s^{-1}$

Subscripts

e = external phase
i = internal phase
n = nth coefficient

Literature Cited

Adamson, A. W., *Physical Chemistry of Surfaces*, Wiley, New York (1990).

Bentley, B. J., and L. G. Leal, "An Experimental Investigation of Drop Deformation and Breakup in Steady Two-Dimensional Linear Flows," *J. Fluid Mech.*, **167**, 241 (1986).

Carriere, C. J., A. Cohen, and C. B. Arends, "Estimation of Interfacial Tension Using Shape Evolution of Short Fibers," *J. Rheol.*, **33**, 681 (1989).

Cohen, A., and C. J. Carriere, "Analysis of a Retraction Mechanism for Imbedded Polymeric Fibers," *Rheol. Acta*, **28**, 223 (1989).

Elemans, P. H. M., J. M. H. Janssen, and H. E. H. Meijer, "The Measurement of Interfacial Tension in Polymer/Polymer Systems: The Breaking Thread Method," *J. Rheol.*, **34**, 1311 (1990).

Joseph, D. D., M. S. Arney, G. Gillberg, H. Hu, D. Hultman, C. Verdier, and H. Vinagre, "A Spinning Drop Tensioextensiometer," *J. Rheol.*, **36**, 621 (1992).

Pozrikidis, C., *Boundary Integral and Singularity Methods for Linearized Viscous Flow*, Cambridge University Press, Cambridge (1992).

Rallison, J. M., and A. Acrivos, "A Numerical Study of the Deformation and Burst of a Viscous Drop in an Extensional Flow," *J. Fluid Mech.*, **89**, 191 (1978).

Rayleigh, Lord, "On the Instability of Jets," *Proc. Lond. Math. Soc.*, **10**, 4 (1878).

Ronay, M., "Determination of the Dynamic Surface Tension of Liquids from the Instability of Excited Capillary Jets and from the Oscillation Frequency of Drops Issued from Such Jets," *Proc. R. Soc. Lond. A*, **361**, 181 (1978).

Rumscheidt, F. D., and S. G. Mason, "Particle Motions in Sheared Suspensions: XII. Deformation and Burst of Fluid Drops in Shear and Hyperbolic Flow," *J. Colloid Sci.*, **16**, 238 (1961).

Stone, H. A., and L. G. Leal, "Relaxation and Breakup of an Initially Extended Drop in an Otherwise Quiescent Fluid," *J. Fluid Mech.*, **198**, 399 (1989).

Tanzosh, J., M. Manga, and H. A. Stone, "Boundary Integral Methods for Viscous Free-Boundary Problems: Deformation of Single and Multiple Fluid-Fluid Interfaces," *Proc. Boundary Element Technologies VII*, Computational Mechanics Publishing, 19 (1992).

Taylor, G. I., "The Formation of Emulsions in Definable Fields of Flow," *Proc. R. Soc. A*, **146**, 501 (1934).

Tjahjadi, M., H. A. Stone, and J. M. Ottino, "Satellite and Subsatellite Formation in Capillary Breakup," *J. Fluid Mech.*, **243**, 297 (1992).

Tomotika, S., "On the Stability of a Cylindrical Thread of a Viscous Liquid Surrounded by Another Viscous Fluid," *Proc. R. Soc. Lond. A*, **150**, 322 (1935).

Manuscript received Apr. 19, 1993, and revision received July 19, 1993.